Satellite Orbit Design and Maintenance for Terrestrial Coverage

Prasenjit Sengupta[*]

Optimal Synthesis Inc., Los Altos, CA 94022

and

Srinivas R. Vadali[†] and Kyle T. Alfriend[‡]

Texas A&M University, College Station, TX 77843

This paper presents semi-analytical techniques for the study of the coverage by satellites in Earth orbits. In particular, the coverage by a satellite over a designated area on the Earth's surface is studied as a function of orbital elements. The semi-analytical nature of the methods developed enable the evaluation of several performance metrics associated with the coverage problem without the need for numerical integration of the orbit's parameters over the satellite's lifetime. Results are shown to match very well with those obtained from numerical simulations on a full-scale model. In the second part of the paper, analytical formulae for velocity increments required for orbit maintenance are presented. These formulae are useful for estimating a fuel budget for a a particular terrestrial coverage mission.

Nomenclature

A	Area of spacecraft cross-section, km^2
a	Semimajor axis, km
C_D	Coefficient of drag

---

[*]Research Scientist, 95 First Street, Suite 240; sengupta@optisyn.com. Member, AIAA.

[†]Stewart & Stevenson - I Professor, Department of Aerospace Engineering, MS 3141; svadali@aero.tamu.edu. Associate Fellow, AIAA.

[‡]TEES Distinguished Research Chair Professor, Department of Aerospace Engineering, MS 3141; alfriend@aero.tamu.edu. Fellow, AIAA.

e	Eccentricity
(E, f, l)	(Eccentric, True, Mean) anomaly, rad
(F, θ, λ)	(Eccentric, True, Mean) arguments of latitude, rad
g	Argument of periapsis, rad
h	Right ascension of the ascending node (RAAN), rad
$\hbar$	Specific angular momentum of the satellite, km^2/s
i	Inclination, rad
$I_{0\ldots3}(x)$	Modified Bessel functions of order 0 to 3, with argument x
J_2	Zonal harmonic coefficient due to Earth oblateness, 1.0826×10^{-3}
m	Mass of spacecraft, kg
n	Mean motion of the satellite in its orbit, rad/s
n_E	Rate of rotation of the Earth about its axis, $7.2921 \times 10^{-5}\mathrm{rad}/s$
p	Semiparameter, km
(q_1, q_2)	Nonsingular components of the eccentricity vector
r	Current radius of the satellite's orbit, km
$R_\oplus$	Radius of the Earth, $6378.1363\,\mathrm{km}$
(u_r, u_θ, u_h)	Components of external acceleration satellite in the rotating frame, km/s^2
β_{half}	Earth-centered half angle of a conical center, rad
Δt	Elapsed time from epoch, s
$(\Delta V_r, \Delta V_\theta, \Delta V_h)$	Velocity impulses in orbit radial, circumferential, and out-of-plane directions
γ_{half}	Sensor half angle of a conical center, rad
κ	Atmospheric scale height, km^{-1}
$\mu_\oplus$	Gravitational parameter of the Earth, $398600.4415\,\mathrm{km}^3/s^2$
ϕ	Latitude, rad
ψ	Longitude, rad
ρ_P	Atmospheric density at perigee, $\mathrm{kg}/\,\mathrm{km}^3$
$\dot{()}_s$	Secular drift rate of orbital angle, rad/s

I.   Introduction

Satellite orbit design for target access, from the point of view of responsive space, is a key area of present-day research. The particular problem studied in this paper is that of the design of orbits for satellites, with the imperative of gaining visual or sensing access to a target on the surface of the Earth. The target could be one location, specified by a latitude or longitude, or a region of interest on the Earth's surface. To this end, the design of the satellite's orbit must satisfy performance metrics that are specified by the end user,

for example, the total time of coverage over a region, access to day-time and night-time coverage, or time required to access a different region, among others. Typically, the design is carried out through the use of numerical tools that simulate the full-scale space environment for low-Earth orbiting satellites.

Several works in the literature[1, 2] study the problem of coverage using repeating-groundtrack or compatible orbits[3], whose orbital period is resonant with the rotation of the Earth and orbit precession, such that the ground trace of the satellite repeats itself after an integral number of orbits of the satellite. These orbits are very useful for mapping the same area multiple times in a given time-frame. However, the use of compatible orbits can result in orbital eccentricities that are significant. Table 1 shows the values for semimajor axis and eccentricity, for the compatibility condition presented in [3], for an orbit inclination of 37°, and with a perigee altitude fixed at 400 km. The conditions for compatibility can be expressed as equations in the mean orbital elements and are presented later in the paper. It can be observed that as the number of repeating groundtracks per day decreases, the value of eccentricity also increases. Some values of repeating groundtracks per day can result in infeasible orbits. For example, as shown in Table 1, for the given perigee altitude and inclination, a requirement of 16 groundtracks per day results in $e = -0.033$.

Table 1. Semimajor Axis and Eccentricity Values for Compatible Orbits

Days	Orbits	a (km)	e
1	12	7997.59	0.152
1	13	7573.33	0.105
1	14	7198.75	0.058
1	15	6864.63	0.012
1	16	N/A	N/A
2	29	7027.12	0.035
3	44	6971.98	0.029
4	59	6944.79	0.023

The drift in perigee is directly related to the eccentricity of the orbit. If the focus of the mission is visual access, altitude from the target site is of importance, and corrective measures have to be taken to maintain perigee. Compatible orbits of lower eccentricity are possible, but due to the nature of the resonance condition, the number of orbits between repeating-groundtracks increases several-fold. After a point, the difference between a compatible orbit with a high order of resonance, and an incompatible orbit, is only one of terminology.

This paper studies the coverage problem using satellites in orbits of low eccentricity. In particular, results are presented for the problem of calculating the time of passage of

a satellite over a given target area. The first approach uses a nonlinear model requiring numerical integration. This provides very accurate results for the time and gain and loss of access. The second method reduces the problem from one requiring numerical integration over the entire lifetime of the orbit, to one requiring a gradient-based numerical solution at the times of gain and loss of access, with the aid of good initial guesses to initiate the root-solving process.

II.   Nonlinear Model

The position of a satellite in its orbit can be obtained by either integrating the equations of motion in an Earth-centered inertial frame (ECI), or a local-vertical local-horizontal (LVLH) frame rotating with the satellite. In the first case, the state variables are the inertial position and inertial velocity. In the second case, the LVLH axes are taken as the satellite's radial direction, the orbit normal, and the cross product completes the triad of vectors. The state variables are the orbital elements, and the equations are given by Gauss' equations[4]:

$$\frac{da}{dt} = \frac{2a^2}{\hbar} \left(e \sin f \, u_r + \frac{p}{r} u_\theta \right) \tag{1a}$$

$$\frac{de}{dt} = \frac{1}{\hbar} \left\{ p \sin f \, u_r + [(p+r)\cos f + re] \, u_\theta \right\} \tag{1b}$$

$$\frac{di}{dt} = \frac{r \cos \theta}{\hbar} u_h \tag{1c}$$

$$\frac{dh}{dt} = \frac{r \sin \theta}{\hbar \sin i} u_h \tag{1d}$$

$$\frac{dg}{dt} = \frac{1}{\hbar e} \left[-p \cos f \, u_r + (p+r)\sin f \, u_\theta \right] - \frac{r \sin \theta \cos i}{\hbar \sin i} u_h \tag{1e}$$

$$\frac{df}{dt} = \frac{\hbar}{r^2} + \frac{1}{\hbar e} \left[p \cos f \, u_r - (p+r)\sin f \, u_\theta \right] \tag{1f}$$

where $\hbar = \sqrt{\mu_\oplus p}$, $p = a(1 - e^2)$, and $r = p/(1 + e \cos f)$. The external accelerations include oblateness and drag effects[5], or, in the case of powered flight, the accelerations due to thrusters. For example, the accelerations due to oblateness effects are given by[5]:

$$\left\{ \begin{array}{c} u_r \\ u_\theta \\ u_h \end{array} \right\} = -\frac{3}{2} \frac{\mu_\oplus J_2 R_\oplus^2}{r^4} \left\{ \begin{array}{c} 1 - 3\sin^2 i \sin^2 \theta \\ 2\sin^2 i \sin \theta \cos \theta \\ 2\sin i \cos i \sin \theta \end{array} \right\} \tag{2}$$

It may be noted that several alternative sets of states can be used to describe satellite motion in the LVLH frame. The equations corresponding to these sets can be obtained directly from Gauss' equations.

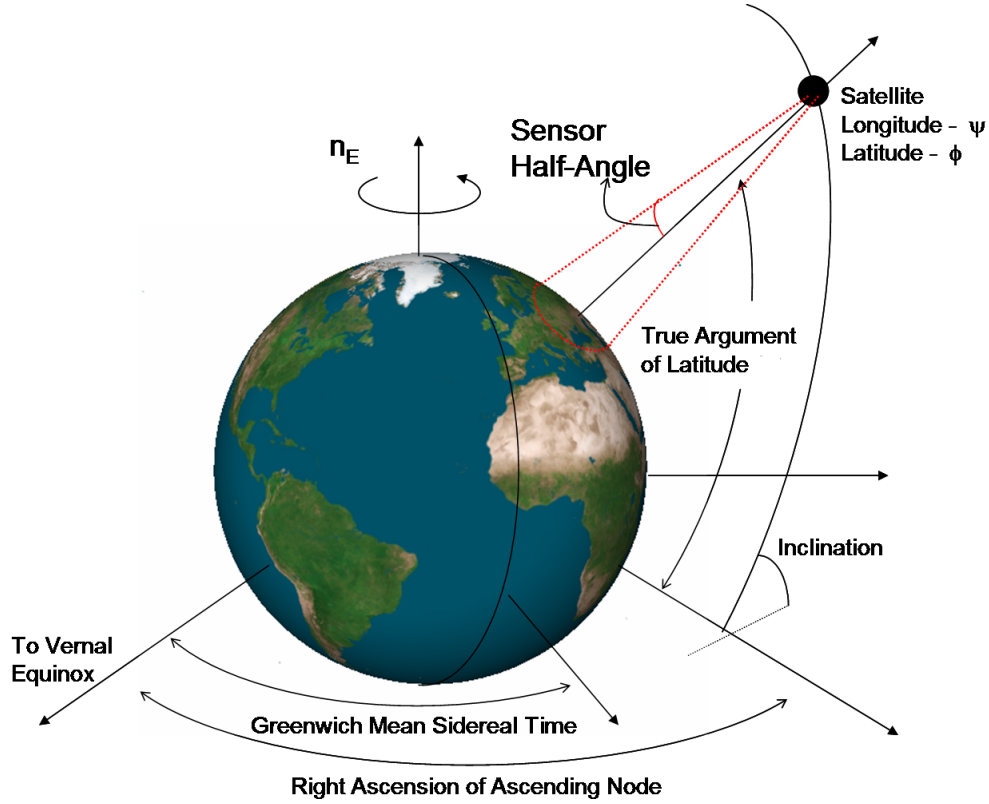A schematic diagram of the satellite in its orbit is shown in Fig. 1. The current latitude

Figure 1. Satellite in an Earth Orbit

and longitude of the satellite in its orbit, and the angle subtended by the conical sensor at the Earth's center, can be obtained by the following equations:

$$\sin\phi = \sin i \sin\theta \tag{3a}$$

$$\psi = g - \text{GMST} - n_E\,\Delta t + \arctan(\cos i \tan\theta) \tag{3b}$$

$$\beta_{\text{half}} = -\gamma_{\text{half}} + \arcsin\left(\frac{r}{R_\oplus}\sin\gamma_{\text{half}}\right) \tag{3c}$$

where GMST is the Greenwich mean sidereal time[3] of epoch. The GMST adjusts the longitude to account for the Greenwich meridian, and the term $n_E\,\Delta t$ accounts for the rotation of the Earth since epoch. Let the latitude and longitude of the target site be denoted by the pair (ψ_0, ϕ_0). The unit vector in the ECI frame, from the origin at the Earth's center, and passing through the target site, is denoted by $\boldsymbol{k}_0$. Similarly, the unit vector from the origin to the satellite is denoted by $\boldsymbol{k}$. These vectors are given by the following equations:

$$\boldsymbol{k}_0 = \{\cos\phi_0\cos\psi_0 \quad \cos\phi_0\sin\psi_0 \quad \sin\phi_0\}^\top \tag{4a}$$

$$\boldsymbol{k} = \{\cos\phi\cos\psi \quad \cos\phi\sin\psi \quad \sin\phi\}^\top \tag{4b}$$

Assuming a conical sensor that covers an area that subtends an angle β_{half} at the Earth's center, the target is considered within access if the angle between the two vectors in Eqs. (4) is less than β_{half}. A conical sensor is assumed to simplify analysis, since any point on the edge of the conical projection on a sphere subtends equal angles with the center of the projection. However, the analysis of different conical projection shapes is also possible, by using a conical sensor whose projection bounds the given projection geometry.

The time at which target access is acquired or lost, can be obtained by checking for the following condition:

$$\boldsymbol{k}_0 \cdot \boldsymbol{k} = \cos \phi$$
$$\Rightarrow \quad \cos \phi \cos \phi_0 \cos(\psi - \psi_0) + \sin \phi \sin \phi_0 = \cos \beta_{\text{half}} \tag{5}$$

If coverage of a target region is desired instead of a target site, then the region can be approximated by a projected circle on the Earth's surface, whose center is given by the pair (ϕ_0, ψ_0), and whose boundary subtends an angle β_0 at the center of the Earth. In this case, Eq. (5) can be used if $\beta_0 + \beta_{\text{half}}$ is used as the argument of the right-hand side.

The time of gain and loss of access to a target site or region can be calculated to the same accuracy as that used to numerically integrate the orbit using Eqs. (1), by using Hénon's method for Poincaré maps[6]. In this method, a new state S is defined, which represents Eq. (5):

$$S = \cos \phi \cos \phi_0 \cos(\psi - \psi_0) + \sin \phi \sin \phi_0 - \cos(\beta_0 + \beta_{\text{half}}) \tag{6}$$

The differential equation for the state can be obtained by differentiating Eq. (6) with respect to time, to obtain:

$$\frac{dS}{dt} = -\sin \phi \cos \phi_0 \cos(\psi - \psi_0)\frac{d\phi}{dt} - \cos \phi \cos \phi_0 \sin(\psi - \psi_0)\frac{d\psi}{dt} + \sin(\beta_0 + \beta_{\text{half}})\frac{d\beta_{\text{half}}}{dt} \tag{7}$$

where, from Eqs. (1) and Eq. (3),

$$\frac{d\phi}{dt} = \frac{1}{\cos \phi}\left(\cos i \sin \theta \frac{di}{dt} + \sin i \cos \theta \frac{d\theta}{dt}\right) \tag{8a}$$

$$\frac{d\psi}{dt} = \frac{dh}{dt} - n_E + \frac{1}{(1 + \cos^2 i \tan \theta)}\left(\sin i \tan \theta \frac{di}{dt} + \cos i \sec^2 \theta \frac{d\theta}{dt}\right) \tag{8b}$$

$$\frac{d\beta_{\text{half}}}{dt} = \frac{\sin \gamma_{\text{half}}}{\sqrt{R_\oplus^2 - r^2 \sin^2 \gamma_{\text{half}}}}\frac{dr}{dt} \tag{8c}$$

Gain or loss of access is triggered when $S = 0$. Equation (6) and Eqs. (1) result in a 7th-order augmented system of equations, comprising the states $\{a \ e \ i \ h \ g \ f \ S\}^{\top}$, which are

integrated until S changes sign, indicating a neighborhood of the time t_0 where $S = 0$. Let the two instants of time be t^- and t^+, and without loss of generality, let it be assumed that $S^- = S(t^-) < 0$, and $S^+ = S(t^+) > 0$. To find the exact time $t_0 \in (t^-, t^+)$ where $S = 0$, a new system of equations, with S as the independent variable, is integrated from $S = S^-$ to $S = 0$, numerically. The new system of equations are obtained by dividing the augmented system by dS/dt. For example, the differential equation for semimajor axis a with respect to S can be derived from Eq. (1a) and Eq. (7) to yield $da/dS = (da/dt)/(dS/dt)$. The 7th equation in the augmented system, given by Eq. (7), is replaced by $dt/dS = (dS/dt)^{-1}$. Upon integration of this system of equations, t_0 can be obtained at $S = 0$.

III.   Model Simplification and Semi-Analytical Approach

The approach in the previous section has two advantages: 1) The accuracy of target acquisition time is the same as that of the integration scheme, and 2) arbitrary perturbations can be added to the model, for example, higher-order zonal harmonics, tesseral and sectorial harmonics, and third-body effects. However, since J_2 and drag dominate these effects in low Earth orbits, considerable simplifications can be introduced in the model, that enable the use of gradient-based root-solving techniques to solve Eqs. (3) directly for the time of target acquisition. These algorithms (for example, the `fsolve` routine of MATLAB®) perform most efficiently with the availability of a good initial guess, and an analytical technique to obtain these guesses, is presented in this section.

A.   Oblateness Effects and Mean Elements

Numerical simulations reveal that the most dominant effects on LEO satellites are due to J_2 and drag. If it is assumed that velocity corrections are routinely applied to correct for drag (discussed later in the paper), then the orbit of the satellite can be described using 'mean' elements obtained from Brouwer theory[7]. Using this theory, the mean semimajor axis, eccentricity and inclination are assumed constant, and the mean RAAN, argument of perigee and mean anomaly change from their initial values at constant secular rates, that are given by

$$\dot{g}_s = -\frac{3}{4}J_2 n \left(\frac{R_\oplus}{p}\right)^2 (1 - 5\cos^2 i) \tag{9a}$$

$$\dot{h}_s = -\frac{3}{2}J_2 n \left(\frac{R_\oplus}{p}\right)^2 \cos i \tag{9b}$$

$$\dot{l}_s = n \left[1 - \frac{3}{4}J_2 \eta \left(\frac{R_\oplus}{p}\right)^2 (1 - 3\cos^2 i)\right] \tag{9c}$$

The current, 'osculating' elements are obtained by a symplectic transformation of the mean elements, by the inclusion of short-periodic and long-periodic variations, of increasing order in J_2. For example, Brouwer[7] and Kozai[8] include terms through $\mathcal{O}(J_2^2)$, whereas [9–12] develop formulae through $\mathcal{O}(J_2^3)$ and $\mathcal{O}(J_2^4)$. Regardless of the order to which the expansions are carried out, the orbital elements at a given time can be obtained directly from Eqs. (9), instead of integrating Eqs. (1) numerically. Depending on the order of desired accuracy, semi-analytic satellite theory[13] can additionally be used generate variations in the orbital elements due to perturbations in the central gravity field. However, in this paper only first order effects due to J_2 are considered.

The mean orbital elements can be used to design compatible orbits, as shown in Table 1. The requirement for resonance between the satellite groundtrack and the Earth's rotation is expressed by the following equation[3]:

$$N_{\text{days}} \left(\dot{l}_s + \dot{g}_s \right) = N_{\text{orbits}} \left(n_E - \dot{h}_s \right) \tag{10}$$

where $N_{\text{orbits}}/N_{\text{days}}$ is the desired number of orbits per day. Furthermore, the constraint on perigee altitude h_p results in the following equation:

$$a(1 - e) = R_\oplus + h_p \tag{11}$$

For given inclination i, Eq. (10) and Eq. (11), together with Eqs. (9), result in one nonlinear equation in either e or a.

B. Solving for Time of Target Access

Although the use of mean elements significantly simplifies analysis, Eqs. (3) are nonlinear, transcendental equations in ϕ and ψ, and apart from the trivial case of an equatorial and circular orbit, cannot be solved in closed form, to obtain Δt, given the target latitude and longitude pair (ϕ_0, ψ_0). Analysis may be simplified if it is assumed that the satellite's orbit is near-circular. In this case, the orbital elements e, g, and the anomalies (E, f, l) are replaced by their nonsingular counterparts $q_1 = e \cos g$, $q_2 = e \sin g$, and $(F, \theta, \lambda) = (E, f, l) + g$. The equivalent of Kepler's equation for nonsingular elements is given by[14]:

$$\sin \theta = \frac{q_1 q_2 \cos F + (1 + \eta - q_1^2) \sin F - (1 + \eta) q_2}{(1 + \eta)(1 - q_1 \cos F - q_2 \sin F)} \tag{12a}$$

$$\cos \theta = \frac{q_1 q_2 \sin F + (1 + \eta - q_1^2) \cos F - (1 + \eta) q_1}{(1 + \eta)(1 - q_1 \cos F - q_2 \sin F)} \tag{12b}$$

$$F - q_1 \sin F + q_2 \sin F = \lambda \tag{12c}$$

In terms of mean elements,

$$\lambda = (g_0 + l_0) + (\dot{g}_s + \dot{l}_s)\Delta t \tag{13a}$$

$$q_1 = q_{10}\cos(\dot{g}_s \Delta t) - q_{20}\sin(\dot{g}_s \Delta t) \tag{13b}$$

$$q_2 = q_{20}\cos(\dot{g}_s \Delta t) + q_{10}\sin(\dot{g}_s \Delta t) \tag{13c}$$

where the subscript '0' is used to denote the initial value of the orbital element.

If eccentricity is assumed low, then only a solution correct to $\mathcal{O}(e)$ may be necessary for an accurate answer. Consequently, the following expansion of the true argument of latitude in terms of the mean argument of latitude is useful:

$$\theta \approx \lambda + 2(q_1 \sin \lambda - q_2 \cos \lambda) \tag{14}$$

Furthermore, terms of order eJ_2 are neglected. It can be seen from Eqs. (13) that q_1 and q_2 time-varying quantities in the presence of oblateness effects; these are held constant at their initial values.

To find repeated points in time for target acquisition by the conical sensor, a large number of initial guesses are required for the inverse solution to Eqs. (3). The solution is obtained in three steps: 1) inverse solution to the latitude access problem, i.e., the time at which the satellite is within the desired latitude, 2) inverse solution to the longitude access problem, i.e., the time at which the satellite is within the desired longitude, and 3) a combination of the two solutions obtained using interval arithmetic.

C. Latitude Access: Restriction to a Ring

This problem is depicted in Fig. 2, where the orbit of the satellite is shown projected on a rotating Earth, and the grid indicates the ring of interest. The maximum Earth-centered half-angle, denoted by $\beta_{\max}$ and maximum swath width of the satellite sensor occur when the satellite is at apogee, $r = a(1 + e)$. From Eq. (3c),

$$\beta_{\max} = -\gamma_{\mathrm{half}} + \arcsin\left(\frac{a(1 + e)}{R_\oplus}\sin\gamma_{\mathrm{half}}\right) \tag{15}$$

The inverse of Eq. (3a) is easily obtained, using the target latitude and longitude pair (ϕ_0, ψ_0), and the maximum half-angle $\beta_{\max}$:

$$\theta_{\mathrm{lim}_{1,2}} = \arcsin\left[\frac{\sin(\phi_0 \mp \beta_{\max})}{\sin i}\right] \tag{16}$$

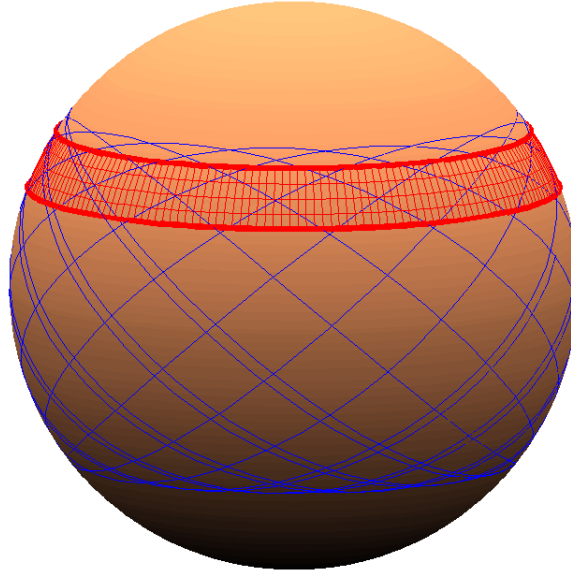Therefore, access to the target region is limited to time segments of the satellite orbit, where

Figure 2. Restriction to a Ring

$\theta_{\text{lim}_1} \leq \theta \leq \theta_{\text{lim}_2}$. The points in time corresponding to these values of true argument of latitude can easily be obtained from the inverse solution to Kepler's equation in nonsingular variables. Future intersections with the target region can be calculated using the satellite orbital period, $\dot{\lambda}_s$.

D. Longitude Access: Restriction to a Sector

The problem of finding the instants of time for access to areas of the same longitude as the target region, is depicted in Fig. 3. As noted earlier, the inverse solution to Eq. (3b) is trivial only for an equatorial, circular orbit. For small values of eccentricity and inclination, a solution can be obtained by a two-step perturbation technique. To simplify analysis, it is assumed that the initial mean argument of latitude, λ_0, is equal to zero at epoch. Analysis on different values of λ_0 can be performed by choosing a different value of the GMST. In general, for long-term orbit analysis, for example, a month or more, the effect of changing λ_0 is large.

The solution to the longitude access problem is divided into two parts. The first part finds an approximate solution for the time (or equivalently, mean argument of latitude) at
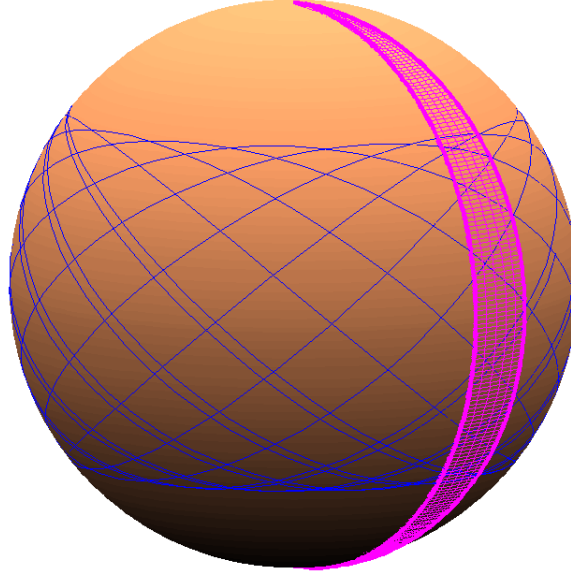
Figure 3. Restriction to a Sector

which the satellite enters (leaves) the sector marked by the minimum (maximum) longitude. It is worth noting that the convention of a satellite entering and leaving a sector at minimum and maximum longitude is valid for prograde orbits only. Analysis in this paper does not change with retrograde orbits. The second part of the method finds time instants of future crossings, once the time of first crossing is known.

If it is first assumed that the orbit is circular, the longitude equation reduces to

$$\text{GMST} + h_0 - \psi_0 + \beta_{\max} + \frac{(\dot{h}_s - n_E)}{\dot{\lambda}_s} \lambda + \arctan(\cos i \tan \lambda) = 0 \qquad (17)$$

Let the variables s_1, s_2, and s_3 be defined as follows:

$$s_0 = \text{GMST} + h_0 - \psi_0 + \beta_{\max} \qquad (18a)$$

$$s_1 = \frac{(\dot{h}_s - n_E)}{\dot{\lambda}_s} \qquad (18b)$$

$$s_2 = \sin i \qquad (18c)$$

Substituting Eqs. (18) in Eq. (17),

$$s_0 + s_1\lambda + \arctan\left(\sqrt{1 - s_2^2}\tan\lambda\right) = 0 \tag{19}$$

When $i = 0$, $s_2 = 0$, and this equation has a straightforward solution, and $s_2 \leq 1$. Let $\lambda = \lambda^{(0)} + s_2\lambda^{(0)} + s_2^2\lambda^{(2)} + \cdots$, and $\chi(s_2) = \arctan(\sqrt{1 - s_2^2}\tan\lambda)$. Upon taking a straightforward expansion[15] in terms of the small parameter s_2, the following equation is obtained:

$$s_0 + s_1\left(\lambda^{(0)} + s_2\lambda^{(1)} + s_2^2\lambda^{(2)} + \cdots\right) + \left(\chi(0) + s_2\left.\frac{d\chi}{ds_2}\right|_{s_2=0} + \frac{s_2^2}{2!}\left.\frac{d^2\chi}{ds_2^2}\right|_{s_2=0} + \cdots\right) = 0 \tag{20}$$

Forming equations from the coefficients of s_2 in Eq. (20), the following are obtained:

$$\lambda^{(1)} = \lambda^{(3)} = \lambda^{(5)} = \ldots = 0$$

$$\lambda^{(0)} = \frac{-s_0}{s_1 + 1}$$

$$\lambda^{(2)} = \frac{\sin 2\lambda^{(0)}}{1!\,2^2\,(s_1 + 1)}$$

$$\lambda^{(4)} = \frac{\sin 2\lambda^{(0)}}{2!\,2^3\,(s_1 + 1)^2}\left[(3s_1 + 1)\sin^2\lambda^{(0)} + (s_1 + 3)\cos^2\lambda^{(0)}\right] \tag{21}$$

$$\lambda^{(6)} = \frac{\sin 2\lambda^{(0)}}{3!\,2^4\,(s_1 + 1)^3}\left[3(5s_1^2 + 4s_1 + 1)\sin^4\lambda^{(0)} + 3(s_1^2 + 4s_1 + 5)\cos^4\lambda^{(0)}\right.$$
$$\left. + 2(5s_1^2 + 22s_1 + 5)\sin^2\lambda^{(0)}\cos^2\lambda^{(0)}\right]$$

$$\lambda^{(8)} = \frac{\sin 2\lambda^{(0)}}{4!\,2^5\,(s_1 + 1)^4}\left[3(35s_1^3 + 47s_1^2 + 25s_1 + 5)\sin^6\lambda^{(0)}\right.$$
$$+ (105s_1^3 + 605s_1^2 + 331s_1 + 63)\sin^4\lambda^{(0)}\cos^2\lambda^{(0)}$$
$$+ (63s_1^3 + 331s_1^2 + 605s_1 + 105)\sin^2\lambda^{(0)}\cos^4\lambda^{(0)}$$
$$\left. + 3(5s_1^3 + 25s_1^2 + 47s_1 + 35)\cos^6\lambda^{(0)}\right]$$

$$\vdots$$

Typically, an expansion to the eighth order in s_2 is sufficient to obtain an accuracy of $1°$ or better, for inclinations up to $60°$. In fact, if $i \geq 45°$, then the following equation may be used:

$$s_0 + s_1\lambda + \arctan\left(s_3\tan\lambda\right) = 0 \tag{22}$$

where $s_3 = \cos i$. For polar orbits, $s_3 = 0$, and $\lambda = -s_0/s_1$. For all other cases, an expansion using s_3 as a small parameter may be employed, such that $\lambda = \lambda^{(0)} + s_3\lambda^{(0)} + s_3^2\lambda^{(2)} + \cdots$.

It can then be shown that:

$$\lambda^{(0)} = -\frac{s_0}{s_1}$$

$$\lambda^{(1)} = -\frac{1}{s_1}\tan\lambda_0$$

$$\lambda^{(2)} = \frac{1}{s_1^2}\frac{\sin\lambda_0}{\cos^3\lambda_0}$$

$$\lambda^{(3)} = \frac{1}{3s_1}\tan^3\lambda_0 - \frac{1}{s_1^3}\frac{\sin\lambda_0(2-\cos^2\lambda_0)}{\cos^5\lambda_0}$$

$$\vdots$$

(23)

The same approach is used to solve for the time of first exit of the sector, using $s_0 = \text{GMST} = h_0 - \psi_0 - \beta_{\max}$.

A similar perturbation approach can be used to obtain the correction $\delta\lambda$, to λ through the first order in eccentricity. It can be shown that

$$\delta\lambda = \frac{-2\cos i \sec^2\lambda(q_{10}\sin\lambda - q_{20}\cos\lambda)}{s_1(1+\cos^2 i \tan^2\lambda) + \cos i \sec^2\lambda} \tag{24}$$

The above formulae result in the calculation of times of first entry and exit into the sector to an accuracy of a few seconds.

The calculation of future crossings into and out of the sector is complicated by the fact that Eq. (3b) has multiple solutions, and the rotation of the Earth must be accounted for. The circular case is considered, and it is assumed that the time of first entry or exit satisfies Eq. (19), with the appropriate value of s for entry or exit. If the next crossing occurs at $\lambda + L$, then this value must also satisfy Eq. (19):

$$s_0 + s_1(\lambda + L) + \arctan\left[\sqrt{1-s_2^2}\tan(\lambda + L)\right] = 0 \tag{25}$$

Subtracting Eq. (19) from Eq. (25), the following equation is obtained:

$$\frac{\tan L}{1 - s_2^2(\sin\lambda + \cos\lambda\tan L)\sin\lambda} = \frac{-\tan s_1 L}{\sqrt{1-s_2^2}} \tag{26}$$

When $s_2 = 0$, $L = L^{(0)} = 2\pi/(1+s_1)$. A complicated solution using perturbation techniques using s_2 as a small parameter may be employed, but this results in solutions that are not only dependent on the inclination, but also on the mean latitude λ. Consequently, an error in calculating the kth crossing compounds the error in calculating λ at the $(k+1)$th crossing. The necessity for a perturbation solution is avoided, if an accurate solution to the prior

crossing is obtained, using numerical optimization. In other words, if λ_{approx} obtained from Eq. (21) and Eq. (24) is used to solve Eq. (19) using gradient techniques, then the accurate value λ thus obtained is used in Eq. (26). Through $\mathcal{O}(s_2^2)$, the following is obtained:

$$L = L^{(0)} - \frac{s_2^2}{2} \frac{\sin 2\lambda \tan^2 L^{(0)} + 2s_1^2 \tan L^{(0)} + \tan s_1 L^{(0)}}{\sec^2 L^{(0)} + s_1 \sec^2 s_1 L^{(0)}} \tag{27}$$

A second order solution is found sufficient, since $L \leq 2\pi$. Since the error contributed by neglecting higher-order inclination terms is high, an eccentricity correction will not improve upon an analytically obtained solution.

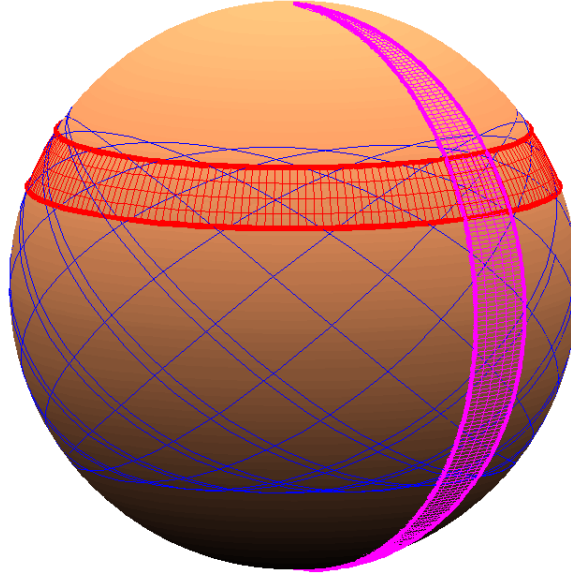## E. Latitude and Longitude Access: Restriction to a Patch

Figure 4. Restriction to a Patch

Although the restriction to the ring latitudes and sector longitudes can be be found independently, resulting in two independent series of time intervals, of interest is the intersection of these two sets. This problem is depicted in Fig. 4.

Let the two sets of time series be denoted by T_{lat} and T_{lon}, such that:

$$T_{\text{lat}} = \bigcup_{j=1}^{m} \left[\alpha_{\text{low}_j}, \alpha_{\text{up}_j} \right] \tag{28a}$$

$$T_{\text{lon}} = \bigcup_{k=1}^{n} \left[\beta_{\text{low}_j}, \beta_{\text{up}_j} \right] \tag{28b}$$

where $[\alpha_{\text{low}_j}, \alpha_{\text{up}_j}]$ is the jth interval of latitude (ring) access, and $[\beta_{\text{low}_j}, \beta_{\text{up}_j}]$ is the kth interval of longitude (sector) access. The intervals of latitude access are mutually disjoint, as are those of longitude access, and are arranged in increasing order, i.e., $\alpha_{\text{low}_{j+1}} > \alpha_{\text{up}_j} \ \forall j$, and $\beta_{\text{low}_{k+1}} > \beta_{\text{up}_k} \ \forall k$. The series of intervals can be rewritten in center-radius form,

$$T_{\text{lat}} = \bigcup_{j=1}^{m} \left\langle \alpha_{c_j}, \alpha_{r_j} \right\rangle \tag{29a}$$

$$T_{\text{lon}} = \bigcup_{k=1}^{n} \left\langle \beta_{c_j}, \beta_{r_j} \right\rangle \tag{29b}$$

where,

$$\alpha_{c_j} = (\alpha_{\text{low}_j} + \alpha_{\text{up}_j})/2, \quad \alpha_{r_j} = (\alpha_{\text{up}_j} - \alpha_{\text{low}_j})/2 \tag{30a}$$

$$\beta_{c_j} = (\beta_{\text{low}_j} + \beta_{\text{up}_j})/2, \quad \beta_{r_j} = (\beta_{\text{up}_j} - \beta_{\text{low}_j})/2 \tag{30b}$$

Let $T = T_{\text{lat}} \cup T_{\text{lon}}$ be the series of $(m + n)$ intervals, whose kth interval is denoted by $< \delta_{c_k}, \delta_{r_k} >$, arranged in increasing order of center value, such that $\delta_{c_{k+1}} \geq \delta_{c_k}$. The kth and $(k+1)$th interval intersect if the distance between their centers is less than the sum of their radii, i.e., if $\delta_{c_{k+1}} - \delta_{c_k} \leq \delta_{r_{k+1}} + \delta_{r_k}$. If the condition of intersection is satisfied, the interval of this intersection is given by

$$\left[\max(\delta_{\text{low}_k}, \delta_{\text{low}_{k+1}}), \min(\delta_{\text{up}_k}, \delta_{\text{up}_{k+1}}) \right] \tag{31}$$

IV. Orbit Maintenance in the Presence of Drag and Oblateness

In the previous section, formulae for analyzing orbital coverage have been presented. The focus of this section is on analytical formulations for the calculation of velocity impulses required for orbit maintenance. Unlike the preceding sections, analysis is not limited to low eccentricity orbits and the results are therefore valid for a larger class of orbits. Situations where orbits may be of moderate eccentricity may be encountered, for example, when compatible orbits are used for coverage, as shown in Table 1.

The major effect of the J_2 perturbation is orbit precession, due to the secular change in the argument of perigee. If the orbit eccentricity is low, this does not pose a significant challenge to orbit design, since the perigee is poorly defined. However, if the orbit eccentricity is moderate, then the observation capabilities of the satellite may suffer, since the perigee is required to stay over a particular region. Atmospheric drag causes a slow decay in the orbit, reducing eccentricity as well as altitude. Hence, periodic re-boosts are necessary for the proper operation of satellites.

In this section, it is assumed that velocity impulses are used to change the orbit parameters. Furthermore, in cases where multiple impulses are required, it is assumed that the intermediate impulses are small and do not change the orbital elements to a large extent, and as a consequence, the initial orbital elements are used in all calculations.

A.   Perigee Maintenance

The change in orbital elements due to velocity impulses can be obtained from Eqs. (1), under the assumption that $\Delta \text{\oe} \approx \dot{\text{\oe}} \, \Delta t$ and $V_i \approx u_i \, \Delta t$, where $\text{\oe}$ is an orbital element, Δt is the duration of the velocity impulse, and i denotes a direction of the LVLH frame. A change in perigee due to a radial and circumferential velocity impulse, is thus given by

$$\Delta g = -\frac{\cos f}{e} \Delta v_r + \frac{\sin f \, (2 + e \cos f)}{e(1 + e \cos f)} \Delta v_\theta \tag{32}$$

where $\Delta v_r = \Delta V_r / \sqrt{\mu_\oplus / p}$ and $\Delta v_\theta = \Delta V_\theta / \sqrt{\mu_\oplus / p}$ are nondimensional quantities. Let the coefficients of Δv_r and Δv_θ be denoted by the components of a vector $\boldsymbol{b} \in \mathbb{R}^{2 \times 1}$, and let Δv_r and Δv_θ be the components of a vector $\boldsymbol{\Delta v} \in \mathbb{R}^{2 \times 1}$. Consequently, Eq. (32) may be rewritten as follows:

$$\Delta g = \boldsymbol{b} \cdot \boldsymbol{\Delta v} \tag{33}$$

For a given Δg, Eq. (33) results in an infinite number of possible solutions for $\boldsymbol{\Delta v}$. The solution space can be constrained by seeking a minimum on the magnitude of the velocity impulse. For a straightforward analytical result, the square of the two-norm of the impulse is minimized; this assumes that one omni-directional in-plane thruster is used. The problem is thus posed as the following:

$$\min \mathcal{J} = \frac{1}{2} ||\boldsymbol{\Delta v}||_2^2 \tag{34a}$$

$$\text{subject to } \Delta g = \boldsymbol{b} \cdot \boldsymbol{\Delta v} \tag{34b}$$

It can be shown that the resulting minimum-norm solution is given by:

$$\Delta \boldsymbol{v}_{\text{min}-\text{norm}} = \frac{\Delta g}{||\boldsymbol{b}||_2^2}\boldsymbol{b} \tag{35}$$

The corresponding cost, denoted by $\mathcal{J}_{\text{min}-\text{norm}}$, is then as follows:

$$
\begin{aligned}
\mathcal{J}_{\text{min}-\text{norm}}(f) &= \frac{1}{2}||\Delta\boldsymbol{v}_{\text{min}-\text{norm}}||_2^2 \\
&= \frac{1}{2}(\Delta g)^2 \frac{e^2(1 + e\cos f)^2}{2e\cos^3 f + (3 - e^2)\cos^2 f - 4e\cos f - 4}
\end{aligned}
\tag{36}
$$

The position where the cost is minimum for a given eccentricity, is symmetric about the apogee and perigee, since $\mathcal{J}_{\text{min}-\text{norm}}(f) = \mathcal{J}_{\text{min}-\text{norm}}(\pi + f)$, $0 \le f < 2\pi$. The appropriate location for applying the impulse can be obtained by minimizing Eq. (36) with respect to f. It can be shown that this requirement results in the solution to the following equation:

$$-e^2 \sin f \left[e^3\cos^4 f + 4e^2\cos^3 f + e(6 + e^2)\cos^2 f + 3(1 + e^2)\cos f + 2e \right] = 0 \tag{37}$$

From a second derivative check of Eq. (36), $f = 0, \pi$ result in maximum cost. Therefore, the minimum cost is obtained from the solution to the following quartic polynomial:

$$P(x) = e^3 x^4 + 4e^2 x^3 + e(6 + e^2)x^2 + 3(1 + e^2)x + 2e = 0 \tag{38}$$

where $x = \cos f$. Only solutions to $P(x)$ such that $x \in \mathbb{R}$, and $|x| \le 1$, are of interest. Since Eq. (38) is a quartic equation, a formula for the solution of interest, given by f^* can be found:

$$
\begin{aligned}
\cos f^* &= -\frac{1}{e} + \frac{1}{e}\left(\frac{\sqrt{4e^6 + 27e^4 - 54e^2 + 27}}{6\sqrt{3}} + \frac{1 - e^2}{2} \right)^{1/3} \\
&\quad -\frac{e}{3}\left(\frac{\sqrt{4e^6 + 27e^4 - 54e^2 + 27}}{6\sqrt{3}} + \frac{1 - e^2}{2} \right)^{-1/3}
\end{aligned}
\tag{39}
$$

Equation (39) results in two positions where the velocity impulse is optimal, f^* and $\pi + f^*$. When e is small,

$$f^* = \frac{\pi}{2} + \frac{2}{3}e + \frac{22}{81}e^3 + \frac{74}{405}e^5 + \mathcal{O}(e^7) \tag{40}$$

and that the corresponding minimum cost is given by:

$$\mathcal{J}_{\text{min}-\text{norm}}^* \approx \frac{e}{12}(6 - e^2)\sqrt{\frac{\mu_\oplus}{p}}\Delta g \tag{41}$$

One problem associated with the use of radial and circumferential velocity increments for perigee correction, is the resultant change in semimajor axis and eccentricity. This change can also be obtained from Eqs. (1), and is given by:

$$\frac{\Delta a}{p} = \frac{2e \sin f}{(1 - e^2)^2} \Delta v_r + \frac{2(1 + e \cos f)}{(1 - e^2)^2} \Delta v_\theta \tag{42a}$$

$$\Delta e = \sin f \, \Delta v_r + \frac{(2 \cos f + e \cos^2 f + e)}{(1 + e \cos f)} \Delta v_\theta \tag{42b}$$

If it is assumed that the change in orbital elements after one impulse is negligible, the optimal impulse for perigee correction can be split into two impulses, one applied at f^*, and the other applied at $\pi + f^*$, each causing a change of $\Delta g/2$. Let the two impulses be denoted by $(\Delta v_{r_1}, \Delta v_{\theta_1})$ and $(\Delta v_{r_2}, \Delta v_{\theta_2})$, and the two corresponding sets of orbital element changes be $(\Delta a_1, \Delta e_1, \Delta g_1)$ and $(\Delta a_2, \Delta e_2, \Delta g_2)$. From Eq. (35), let the two velocity impulses be selected such that

$$\Delta v_{r_1} = \Delta v_{r_2} = \frac{e \cos f^*(1 + e \cos f^*)^2}{2e \cos^3 f^* + (3 - e^2) \cos^2 f^* - 4e \cos f^* - 4} \left(\frac{\Delta g}{2} \right) \tag{43a}$$

$$\Delta v_{\theta_1} = -\Delta v_{\theta_2} = \frac{-e \sin f^*(1 + e \cos f^*)(2 + e \cos f^*)}{2e \cos^3 f^* + (3 - e^2) \cos^2 f^* - 4e \cos f^* - 4} \left(\frac{\Delta g}{2} \right) \tag{43b}$$

The two impulses are applied at f^* and $\pi + f^*$, respectively. Since $\cos f^* = \cos(\pi + f^*)$ and $\sin f^* = -\sin(\pi + f^*)$, Eq. (32) and Eqs. (42) can be used to show that:

$$\Delta g_1 + \Delta g_2 = \Delta g \tag{44a}$$

$$\Delta a_1 + \Delta a_2 = 0 \tag{44b}$$

$$\Delta e_1 + \Delta e_2 = 0 \tag{44c}$$

A change in perigee can also be caused by an out-of-plane impulse, ΔV_h, as can be seen from Eqs. (1). An out-of-plane impulse may be required to correct for drift in RAAN, given by the following equation:

$$\Delta h = \frac{\sin \theta}{\sin i \, (1 + e \cos f)} \Delta v_h \tag{45}$$

where $\Delta v_h = \Delta V_h / \sqrt{\mu_\oplus / p}$. An out-of-plane impulse also causes a change in orbit inclination, given by:

$$\Delta i = \frac{\cos \theta}{(1 + e \cos f)} \Delta v_h \tag{46}$$

Therefore, the out-of-plane impulse should be applied at $\theta = \pi/2$ to avoid inclination change.

This causes a change $\Delta g = -\sin\theta\cot i/(1+e\cos f)\Delta v_h$, that can be corrected using in-plane impulses.

B.   Orbit Maintenance in the Presence of Drag

In this section, the effects of drag are studied on the satellite orbit. A simplified analysis is performed to get approximate values for the amount of fuel (velocity impulse) required to correct for drag, by the use of analytical formulae. The assumptions are as follows:

1. No oblateness effects: Since oblateness effects have been accounted for in the orbit design procedure, no fuel is necessary to correct for drift arising due to J_2. Furthermore, it is also assumed that the effect of drag is corrected for, periodically; therefore the change in orbital elements due to drag are assumed not to change the secular drift rates due to J_2.

2. A non-rotating atmosphere with an exponential pressure equation is assumed. In this case, the only changes are in the semimajor axis, eccentricity, and argument of periapsis. Furthermore, only the semimajor axis and eccentricity exhibit secular growth.

3. A spherical satellite is assumed, to simplify drag formulation.

This section draws on previous works by Jacchia[16], King-Hele[17], and Mishne[18]. Reference [18] shows that the change in the semimajor axis and eccentricity per orbit, due to drag effects, are given by

$$
\begin{aligned}
\Delta a &= -2\rho_P a^2 (2\pi) K_d \left[I_0(\kappa ae) + 2e I_1(\kappa ae) \right. \\
&\left. + (3e^2/4)\left\{ I_0(\kappa ae) + I_2(\kappa ae) \right\} \right] \exp(-\kappa ae) \quad (47\text{a}) \\
\Delta e &= \rho_P a(2\pi) K_d \left[2I_1(\kappa ae) + e\left\{ I_0(\kappa ae) + I_2(\kappa ae) \right\} \right. \\
&\left. - (e^2/4)\left\{ 5I_1(\kappa ae) + I_3(\kappa ae) \right\} \right] \exp(-\kappa ae) \quad (47\text{b})
\end{aligned}
$$

where

$$
K_d = \frac{AC_D}{2m} \quad (48)
$$

As noted in [18], the average change in g due to atmospheric drag is zero. Equations (47) are correct through $\mathcal{O}(e^2)$. From Eqs. (42), the velocity increments required for given changes in semimajor axis and eccentricity Δa and Δe are given as follows:

$$
\Delta v_r = -\frac{\eta^2}{2}\frac{(e + 2\cos f + e\cos^2 f)}{\sin f}\frac{\Delta a}{p} + \frac{(1 + e\cos f)^2}{\eta^2 \sin f}\Delta e \quad (49\text{a})
$$

$$\Delta v_\theta = \frac{\eta^2}{2}(1 + e\cos f)\frac{\Delta a}{p} - \frac{e}{\eta^2}(1 + e\cos f)\,\Delta e \tag{49b}$$

However, depending upon the location of the impulse, i.e., depending on the value of true anomaly where the impulse is applied, the magnitude can vary significantly. For example, it is immediately apparent that applying the impulse near apogee or perigee will lead to very high values for the radial velocity impulse Δv_r. Furthermore, the use of one impulse may not be efficient, since the semimajor axis and eccentricity are optimally corrected at individually different locations in the orbit. Therefore, it may be more beneficial to use two or more impulses, and avoid the use of radial impulses. Assuming two circumferential impulses are used, Eq. (42) are modified as follows:

$$\frac{\Delta a}{p} = \frac{2(1 + e\cos f_1)}{(1 - e^2)^2}\Delta v_{\theta_1} + \frac{2(1 + e\cos f_2)}{(1 - e^2)^2}\Delta v_{\theta_2} \tag{50a}$$

$$\Delta e = \frac{(2\cos f_1 + e\cos^2 f_1 + e)}{(1 + e\cos f_1)}\Delta v_{\theta_1} + \frac{(2\cos f_2 + e\cos^2 f_2 + e)}{(1 + e\cos f_2)}\Delta v_{\theta_2} \tag{50b}$$

The desired impulses can be found from the inverse solution to Eqs. (50). Since Eqs. (47) are correct through $\mathcal{O}(e^2)$, the values of the impulses are expanded through $\mathcal{O}(e^2)$, to yield the following expressions:

$$
\begin{aligned}
\Delta v_{\theta_1} =\ & \frac{1}{8(\cos f_2 - \cos f_1)}\Bigg[-(e^2\cos^2 f_1\cos f_2 - 2e\cos f_1\cos f_2 + 6e^2\cos f_2 \\
& -4\cos f_2 - e^2\cos f_1 - 2e)\frac{\Delta a}{p} - (2e^2\cos f_1\cos f_2 + 4e\cos f_2 - e^2\cos^2 f_1 \\
& +2e\cos f_1 + 3e^2 + 4)\,\Delta e\Bigg]
\end{aligned}
\tag{51a}
$$

$$
\begin{aligned}
\Delta v_{\theta_2} =\ & \frac{1}{8(\cos f_2 - \cos f_1)}\Bigg[(e^2\cos f_1\cos^2 f_2 - 2e\cos f_1\cos f_2 + 6e^2\cos f_1 \\
& -4\cos f_1 - e^2\cos f_2 - 2e)\frac{\Delta a}{p} + (2e^2\cos f_1\cos f_2 + 4e\cos f_1 - e^2\cos^2 f_2 \\
& +2e\cos f_2 + 3e^2 + 4)\,\Delta e\Bigg]
\end{aligned}
\tag{51b}
$$

The cost associated with the impulses given by Eqs. (51) is dependent on the choice of f_1 and f_2. The behavior of cost with respect to the choice of f_1 and f_2 is difficult to analyze, although it may be studied numerically. It may be observed, however, that if f_1 is known, then a cost function $\mathcal{J}_{\text{drag}} = (\Delta v_{\theta_1}^2 + \Delta v_{\theta_2}^2)/2$ can be formed, such that $d\mathcal{J}_{\text{drag}}/df_2 = 0$ results in a quartic equation in $\cos f_2$ that can be solved. Similarly, if f_2 is known, $d\mathcal{J}_{\text{drag}}/df_1 = 0$

results in a quartic equation $\cos f_1$. By selecting roots of the quartic polynomials such that additional constraints $0 \leq f_1 \leq \pi$ and $\pi \leq f_2 \leq 2\pi$ are satisfied, the equations can be solved by iteration until convergence to optimal locations f_1^* and f_2^*. The quartic polynomials are presented as an appendix.

V. Numerical Results

A. Comparison of Numerical and Semi-analytical Results

The basic design criteria for the results are as follows. A target site in the Mediterranean Sea is located, with a latitude of 37°N, and longitude of 14°E (this corresponds roughly to the location of the island of Sicily). A satellite is placed into a near-circular orbit at epoch date November 1, 2006, with initial mean elements $a = 6812.2 \, \text{km}$, $e = 0.005$, $i = 37°$, and $h_0 = 30°$. Up to three months of the satellite's lifetime is studied; since the number of times the satellite orbits around the planet is large, the initial value of the argument of periapsis and mean anomaly make insignificant contribution to the results, and are assumed zero.

Table 2. Coverage Time

Days	Total Access, Analytical (min.)	Total Access, Numerical (min.)	Daytime Access, Analytical (min.)	Daytime Access, Numerical (min.)
29	460.6	461.6	174.8	174.5
58	940.7	943.1	367.3	367.0
91	1477.4	1483.1	608.9	611.1

The satellite sensor is assumed to be conical with a sensor half-angle of 40°. Table 2 presents comparisons between the results from numerical integration, assuming a model with the J_2 perturbation included, and the results from the semianalytical technique presented in this paper. The orbit of the satellite is integrated over varying lengths of time, as shown in the first column using a 7th-order Runge-Kutta-Fehlberg integration formula[20] with an 8th-order correction. Consequently, the time of access is calculated with the same accuracy as the integration tolerance. Although numerical integration schemes for the specific purpose of orbit propagation are well-represented in the literature[21], this paper does not explore their use since the methods developed can be suitably adapted to any scheme with ease.

The results from numerical integration and semianalytical root-solving are presented in the second and third columns, and it is shown that the results match within an error of six minutes over a three month period. The deviation between the two results is due to the fact that the seminanalytical technique chosen is correct to the first order in only. However, the

calculation of time of access based on the semianalytical technique results in a saving of over 70% in computation time.

If a measure of daylight coverage is also desired, then it is easy to select those time intervals of coverage that occur in local daylight time. In this case, daylight is assumed to occur between 0700hrs and 1700hrs. These results are useful in the case of multiple sensors for different wavelengths.

## B.   Coverage Variation with Launch Parameters

Among the orbital elements, a low value of eccentricity is desired, and the semimajor axis is fixed if a constraint on perigee altitude is present. The initial values of argument of perigee and mean anomaly are not important; as a result, the inclination and RAAN offer some freedom of choice for orbit design.

Figures 5(a) and 5(b) show the time of coverage for different values of initial RAAN, adjusted for the GMST, and for inclinations varying from 35° to 39°. For different epoch time, the graph will either shift leftwards or rightwards, due to a change of GMST. The mean semimajor axis and eccentricity are 6812 km and 0.005, respectively, which is the same as the previous example. It is observed that the total time of coverage is not very sensitive to initial RAAN; resulting in a difference of 0.5 minute extra coverage time per day, depending on initial RAAN. However, maximum coverage is obtained for an inclination of 38°, as shown by the dotted line. Approximately 17 minutes of coverage per day, is obtained at this eccentricity. This value of inclination confirms results presented in [19], where it is suggested that the inclination of a satellite observing a region be selected within 1° of the maximum latitude of observation. Figure 5(b) shows that if the initial RAAN adjusted for GMST is in the range $-30° \leq h_0 \leq 60$, then daylight coverage is minimum, at less than 2 minutes per day. However, as the total time of the mission increases, the sensitivity of daylight coverage to RAAN diminishes. The variation of daytime coverage with mission length is shown in Fig. 6.

It is observed from Fig. 6 that the for the first and third month of the orbit's lifetime, daytime coverage shows variation with launch RAAN adjusted for GMST. For the second month, there is almost no variation. Simulations also show that daytime coverage shows variation in every odd month, and the variation decreases as time elapses. This is due to the precessing nature of the orbit in the Earth's rotating frame; the satellite tends to equalize night-time coverage and day-time coverage over sufficiently long periods of time. Therefore, depending on the type and length of mission, Fig. 6 is a good indicator for the initial launch conditions suitable for the maximization of daytime coverage.
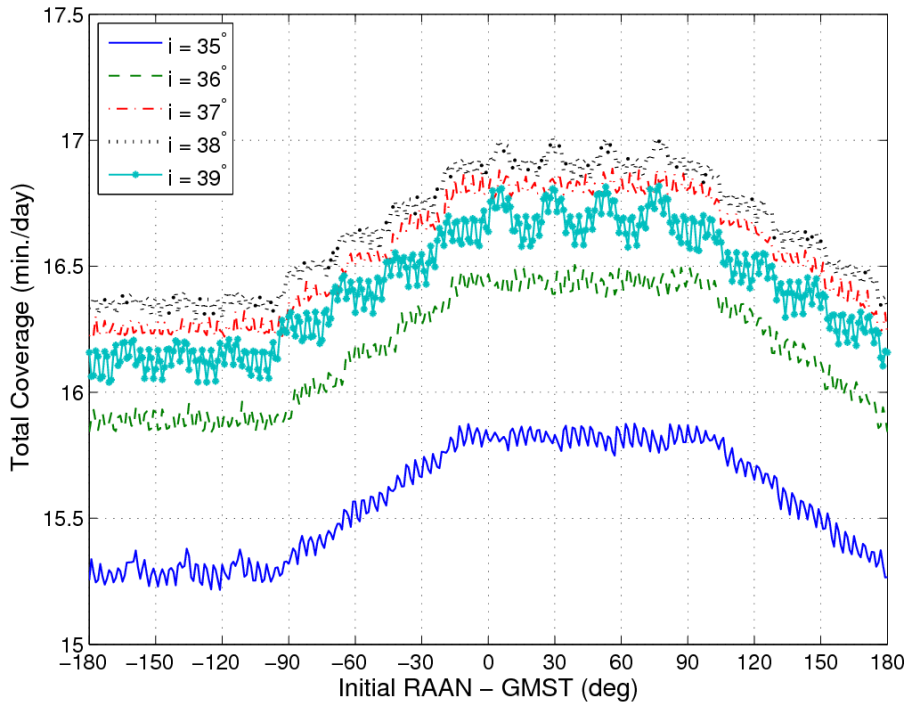
(a) All Day
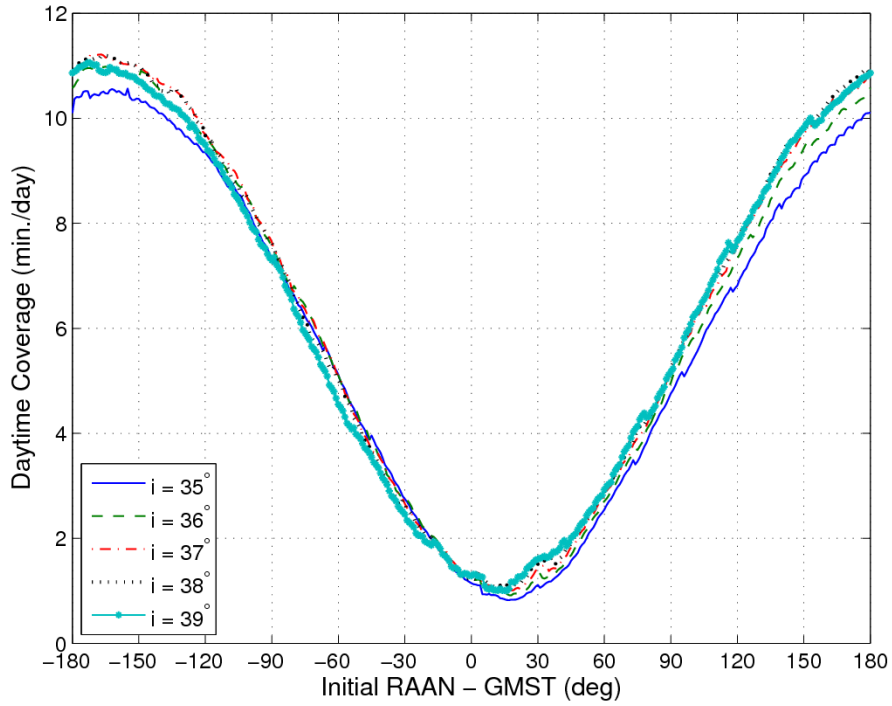
(b) Daytime

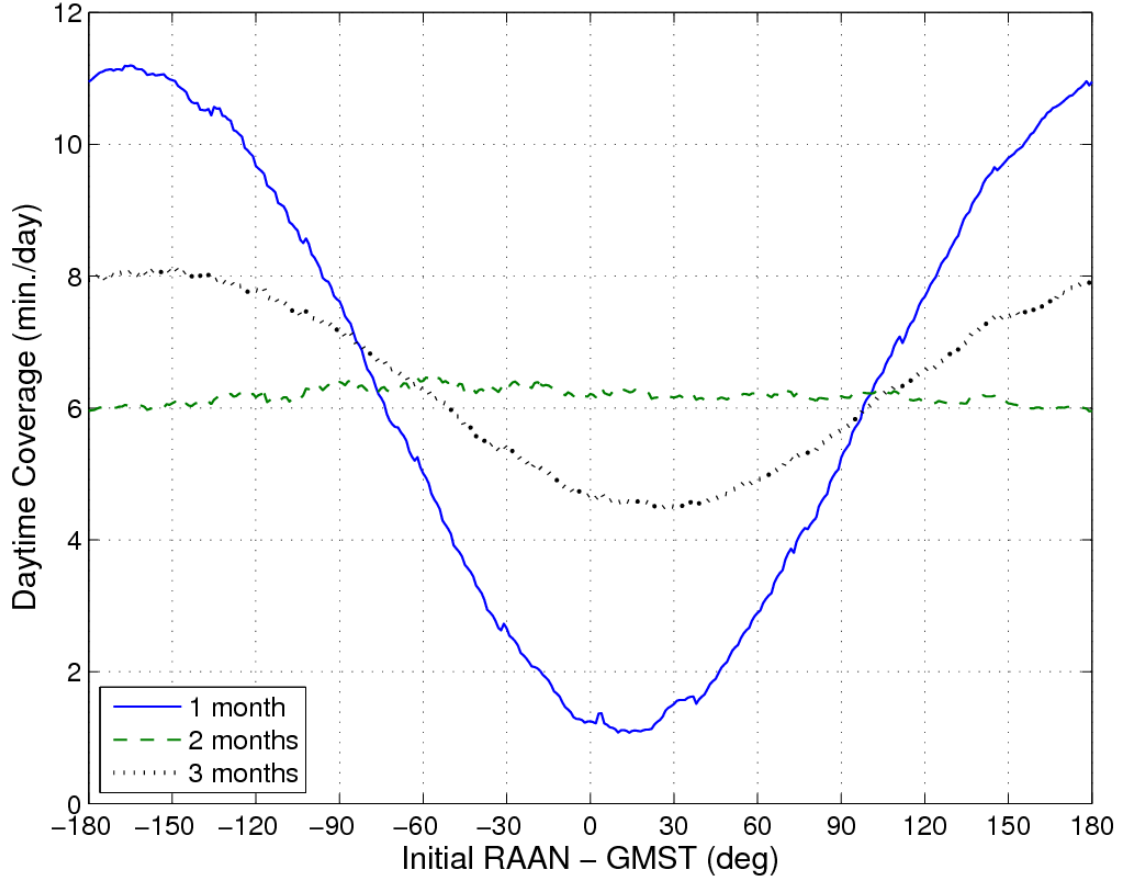**Figure 5. Coverage Statistics Over a 29 Day Period**

**Figure 6. Variation of Daytime Coverage with Elapsed Time**

C. Orbit Maintenance in the Presence of Drag

To analyze the effects of drag, it is first necessary to define the physical parameters of the satellite. It is assumed that the satellite has mass $m = 100\,\text{kg}$, cross-section area $A = 1 \times 10^{-6}\,\text{km}^2$, and coefficient of drag $C_D = 2.2$. The atmospheric values are presented in [17], and are selected as $\rho_P = 7 \times 10^{-3}\,\text{kg/km}^3$, $H = 40\,\text{km}$, and $\kappa = 1/H$.

Consider an orbit with an inclination $i = 38°$, and $h_0 = g_0 = l_0 = 0°$. Perturbation effects are not considered, since inclusion of these effects only results in periodic variations in semimajor axis and eccentricity, and drag causes secular drift. Figures 7 show the effects of drag on semimajor axis, eccentricity, and velocity increment required to reboost the orbit to its original elements, after a month (28 days), respectively. The figures show results for two values of perigee altitude, 400 km and 450 km, depicted by the solid and broken lines, respectively, and for apogee altitude varying from 450 km to 600 km, respectively. The case where perigee altitude is 400 km and apogee altitude is 450 km is representative of the examples in the previous sections. Figure 7(a) shows that for circular orbits, drag effects result in the maximum decrease of semimajor axis (approximately 20 km) over a month. As
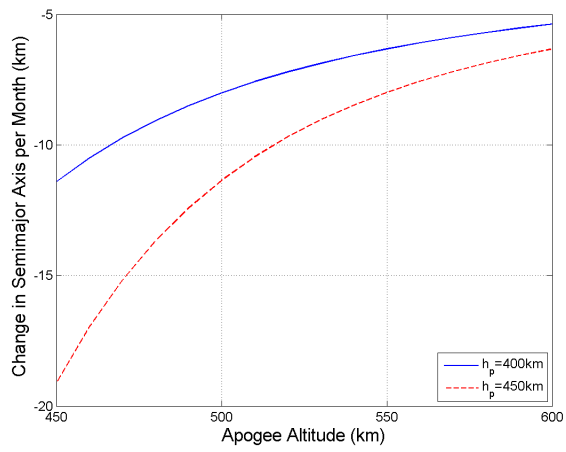
(a) Change in Semimajor Axis
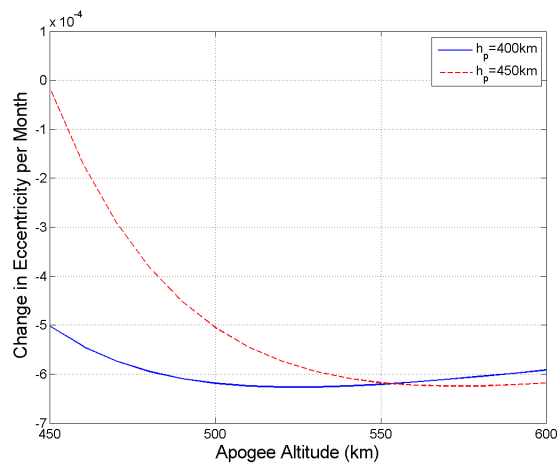
(b) Change in Eccentricity
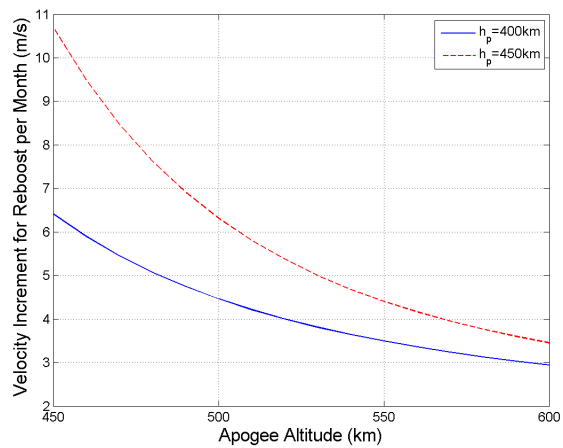
(c) Velocity Increments for Drag Correction

Figure 7. Drag Effects on Semimajor Axis, Eccentricity, and Velocity Increments

eccentricity increases, the satellite spends a larger proportion of time in regions further from the Earths surface, and is less prone to drag effects. While drag effects on semimajor axis are shown to be monotonic, this is no longer the case with the eccentricity of the orbit, as shown in Figure 7(b). It should be noted that the maximum eccentricity considered in these figures is approximately 0.015, which is well within the ambit of the theory used for drag studies. The values agree closely with those obtained from simulation software such as SOAP®under similar conditions.

Figure 7(c) shows the velocity increment required for orbit reboost due to drag effects. Use of Eqs. (49) is made here, to calculate the magnitude of the velocity impulse required. For the nominal example, the velocity increment required to account for drag effects is approximately 6.5 m/s/month. For other cases, as shown in Fig. 7(c), this can be as high as 11 m/s/month, or as low as 2.5 m/s/month. If two impulses are used, then Eqs. (52) can be used to find the magnitude of velocity impulse required. The use of two impulses, under the assumption that radial impulses are not used, and the orbit is nearly circular, results in a fuel cost approximately half of what is shown in Fig. 7(c). This analysis is therefore very useful for the study of fuel budgets for missions of this class.

VI.   Conclusions

In this paper, the problem of time for target access has been analyzed. Two methods have been presented to calculate the start of end time of target access by a satellite with a conical sensor. The first method requires numerical integration and provides accurate results, and can include arbitrary perturbation effects. The second method simplifies the approach and reduces the problem to the inverse solution to transcendental equations. Analytical techniques are employed to obtain initial guesses, that can solve these equations. Comparisons with numerical integration show very accurate results. Furthermore, analytical formulae for orbit maintenance in the presence of drag and oblateness are presented that are useful for estimating fuel budgets.

Appendix: Development of Auxiliary Equations for Drag Correction Using Velocity Impulses

Let $\mathcal{J}_{\text{drag}} = (\Delta v_{\theta_1}^2 + \Delta v_{\theta_2}^2)/2$ where $\Delta v_{\theta_1} \equiv \Delta v_{\theta_1}(f_1, f_2)$ and $\Delta v_{\theta_2} \equiv \Delta v_{\theta_2}(f_1, f_2)$ are given by Eqs. (51). Let $x = \cos f_1$ and $y = \cos f_2$, and let $l_1 = \Delta a/p$ and $l_2 = \Delta e$. Equations (51) can be rewritten as follows:

$$\Delta v_{\theta_1} = \frac{1}{8(x - y)} \left\{ \left[e^2 \left(x^2 y + 6y - x \right) - 2e \left(xy + 1 \right) - 4y \right] l_1 \right.$$

$$+ \left[e^2 \left(2xy - x^2 + 3\right) + 3e \left(2y + x\right) + 4\right] l_2\} \tag{52a}$$

$$\Delta v_{\theta_2} \;=\; \frac{1}{8(y-x)} \left\{ \left[e^2 \left(xy^2 + 6x - y\right) - 2e \left(xy + 1\right) - 4x\right] l_1 \right.$$

$$\left. + \left[e^2 \left(2xy - y^2 + 3\right) + 2e \left(2x + y\right) + 4\right] l_2 \right\} \tag{52b}$$

Let $c_{0\ldots4}(z)$ be defined as follows:

$$c_4(z) \;=\; e^4(l_1 z - l_2)^2 \tag{53a}$$

$$c_3(z) \;=\; -e^2(l_1 z - l_2)(3e^2 l_1 z^2 + 3e^2 l_1 - 2l_1 - 2e^2 l_2 z + 2el_2) \tag{53b}$$

$$c_2(z) \;=\; 3e^2 z(l_1 z - l_2)(e^2 l_1 z^2 + 3e^2 l_1 - 2l_1 + 2el_2) \tag{53c}$$

$$c_1(z) \;=\; -\left(e^4 l_1^2 z^5 + 9e^4 l_1^2 z^3 - 2e^2 l_1^2 z^3\right.$$

$$-12e^3 l_1^2 z^2 + 12el_1^2 z^2 + 8e^4 l_1^2 z - 12e^2 l_1^2 z + 8l_1^2 z - 4e^3 l_1^2 + 4el_1^2 + l_2 e^4 l_1 z^4$$

$$-10e^3 l_1 l_2 z^3 + 15e^4 l_1 l_2 z^2 - 42e^2 l_1 l_2 z^2 + 16e^3 l_1 l_2 z - 40el_1 l_2 z + 8e^4 l_1 l_2$$

$$-8e^2 l_1 l_2 - 8l_1 l_2 + 14e^4 l_2^2 z^3 + 42e^3 l_2^2 z^2 + 16e^4 l_2^2 z + 48e^2 l_2^2 z$$

$$\left. +16e^3 l_2^2 + 16el_2^2\right) \tag{53d}$$

$$c_0(z) \;=\; 3e^4 l_1^2 z^4 - 2e^2 l_1^2 z^4 + 4e^3 l_1^2 z^3 - 4el_1^2 z^3 - 8e^4 l_1^2 z^2$$

$$+12e^2 l_1^2 z^2 - 8l_1^2 z^2 + 12e^3 l_1^2 z - 12el_1^2 z - 4e^2 l_1^2 + e^4 l_1 l_2 z^5 + 2e^3 l_1 l_2 z^4$$

$$-11e^4 l_1 l_2 z^3 + 18e^2 l_1 l_2 z^3 - 16e^3 l_1 l_2 z^2 + 40el_1 l_2 z^2 - 24e^4 l_1 l_2 z + 24e^2 l_1 l_2 z$$

$$+24l_1 l_2 z + 16e^3 l_1 l_2 + 16el_1 l_2 - e^4 l_2^2 z^4 - 18e^3 l_2^2 z^3 - 16e^4 l_2^2 z^2$$

$$-48e^2 l_2^2 z^2 - 48e^3 l_2^2 z - 48el_2^2 z - 16e^4 l_2^2 - 32e^2 l_2^2 - 16l_2^2 \tag{53e}$$

If x is assumed known, then $d\mathcal{J}_{\mathrm{drag}}/dy = 0$ results in the following equation:

$$\varphi_1(y) \;=\; c_4(z)\, y^4 + c_3(z)\, y^3 + c_2(z)\, y^2 + c_1(z)\, y + c_0(z) = 0 \tag{54}$$

Similarly, if y is assumed known, $d\mathcal{J}_{\mathrm{drag}}/dx = 0$ results in another quartic equation $\varphi_2(x)$, given by:

$$\varphi_2(x) \;=\; c_4(y)\, x^4 + c_3(y)\, x^3 + c_2(y)\, x^2 + c_1(y)\, x + c_0(y) = 0 \tag{55}$$

Since $\varphi_1(y)$ and $\varphi_2(x)$ are quartic equations, their roots can be found through analytical formulae. Only roots that satisfy the conditions $x, y \in \mathbb{R}$, $-1 \le x \le 1$, and $-1 \le y \le 1$ are to be selected. These equations can be solved by iteration to yield the optimal values of f_1 and f_2 for impulse application.

References

[1] Aorpimai, M. and Palmer, P. L., "Repeat-Groundtrack Orbit Acquisition and Maintenance for Earth-Observation Satellites," *Journal of Guidance, Control, and Dynamics*, Vol. 30, No. 3, May-June 2007, pp. 786–793.

[2] Abdelkhalik, O. and Mortari, D., "Two-Way Orbits," *Celestial Mechanics and Dynamical Astronomy*, Vol. 94, No. 4, April 2006, pp. 399–410.

[3] Vallado, D. A., *Fundamentals of Astrodynamics and Applications*, Microcosm, Inc., El Segundo, CA, 2nd ed., 2001.

[4] Battin, R. H., *An Introduction to the Mathematics and Methods of Astrodynamics*, AIAA Education Series, American Institute of Aeronautics and Astronautics, Inc., Reston, VA, revised ed., 1999.

[5] Kechichian, J. A., "Motion in General Elliptic Orbit with Respect to a Dragging and Precessing Coordinate Frame," *The Journal of the Astronautical Sciences*, Vol. 46, No. 1, January-March 1998, pp. 25–46.

[6] Hénon, M., "On the Numerical Computation of Poincaré Maps," *Physica D: Nonlinear Phenomena*, Vol. 5, No. 2-3, September 1982, pp. 412–414.

[7] Brouwer, D., "Solution of the Problem of Artificial Satellite Theory without Drag," *The Astronomical Journal*, Vol. 64, November 1959, pp. 378–397.

[8] Kozai, Y., "The Motion of a Close Earth Satellite," *The Astronomical Journal*, Vol. 64, November 1959, pp. 367–377.

[9] Déprit, A. and Rom, A., "The Main Problem of Artificial Satellite Theory for Small and Moderate Eccentricities," *Celestial Mechanics*, Vol. 2, No. 2, July 1970, pp. 166–206.

[10] Aksnes, K., "A Note on 'The Main Problem of Artificial Satellite Theory for Small Eccentricities, By A. Déprit and A. Rom, 1970," *Celestial Mechanics*, Vol. 4, No. 1, September 1971, pp. 119–121.

[11] Déprit, A., "The Main Problem of Artificial Satellites to Order Four," *Journal of Guidance, Control, and Dynamics*, Vol. 4, No. 2, March-April 1981, pp. 201–206.

[12] Coffey, S. L. and Déprit, A., "Third-Order Solution to the Main Problem of Satellite Theory," *Journal of Guidance, Control, and Dynamics*, Vol. 5, No. 4, July-August 1982, pp. 366–371.

[13] Danielson, D. A., Neta, B., and Early, L. W., "Semianalytic Satellite Theory (SST): Mathematical Algorithms," Tech. Rep., Department of Mathematics, Naval Postgraduate School, January 1994.

[14] Gim, D.-W. and Alfriend, K. T., "State Transition Matrix of Relative Motion for the Perturbed Noncircular Reference," *Journal of Guidance, Control, and Dynamics*, Vol. 26, No. 6, November-December 2003, pp. 956–971.

[15] Nayfeh, A. H., *Perturbation Methods*, John Wiley & Sons, Inc., New York City, NY, 1973.

[16] Jacchia, L. G., "New Static Models of the Thermosphere and Exosphere with Empirical Temperature Profiles," Tech. Rep. SAO Special Report 313, Smithsonian Astrophysical Observatory, May 1970.

[17] King-Hele, D. G., *Satellite Orbits in an Atmosphere: Theory and Applications*, Blackie and Son, Ltd., London, United Kingdom, 1987.

[18] Mishne, D., "Formation Control of Satellites Subject to Drag Variations and J_2 Perturbations," *Journal of Guidance, Control, and Dynamics*, Vol. 27, No. 4, July-August 2004, pp. 685–692.

[19] Wertz, J. R., "Coverage, Responsive, and Accessibility for Various 'Responsive Orbits'," *3rd Responsive Space Conference*, Los Angeles, CA, 2005, April 2005, Paper RS-2005-2002.

[20] Fehlberg, E., "Classical Fifth, Sixth, Seventh, and Eighth Order Runge Kutta Formulas with Stepsize Control," Tech. Rep. NASA TR R-287, 1968.

[21] Berry, M. M. and Healy, L. M., "Implementation of Gauss-Jackson Integration for Orbit Propagation," *The Journal of the Astronautical Sciences*, Vol. 52, No. 3, July-September 2004, pp. 331–357.